Progress In Electromagnetics Research C, Vol. 53, 1–10, 2014

Ultra-Wideband (UWB) Differential-Fed Antenna with Improved Radiation Patterns

Junhui Wang* **and Yingzeng Yin**

Abstract—This study proposes a differential-fed microstrip antenna, which is characterized with an ultra-wideband of 120% (3–12 GHz), improved radiation patterns, stable gains, and compact size. Two symmetrical trapezoid shaped slots and four triangle-cut corners on the ground are used to improve the impedance matching over the UWB frequency band. To clarify the improved radiation characteristics, the simulated radiation patterns of the proposed antenna are compared with the conventional single-ended feed UWB antennas. The measured results show that, in the entire frequency band, the designed antenna exhibits a stable radiation patterns and the gain variation is less than 2 dB. Furthermore, the polarization purity are increased compared with the conventional ones, especially in the high frequency band.

1. INTRODUCTION

Due to the advantages of high date rate, great capacity, simplicity, and low cost, ultra-wideband (UWB) short-range wireless technology has been paid more and more attention since the Federal Commercial Commission (FCC) released the frequency band 3.1–10.6 GHz for commercial UWB systems [1]. As an important component of the UWB system, the UWB antenna is required to have the features of simple structure, wide impedance bandwidth (BW), easy integration, stable radiation patterns, and constant gain in the desired direction. Planar antenna, due to its excellent advantages of compact size and easy integration with RF circuits, is one of the most attractive candidates for UWB antennas. So far to now, various planar UWB antennas have been presented, such as circular monopole antenna [2], rectangular aperture antenna [3], open slot antenna [4], fractal bow-tie dipole antenna [5], multi-mode slotline antenna [6], self-complementary antenna [7], and so on. Although these types of antennas can be easily matched over the UWB band, there exists a common deficiency of deterioration of radiation pattern. The radiation patterns of these antennas deviate from the broadside direction in the high frequency band (above 9 GHz), which may cause the mistake for UWB applications that require stable radiation pattern [8, 9]. To alleviate this problem, several techniques have been proposed to improve the radiation pattern of the UWB antenna. In [10], the mushroom-like electromagnetic band-gap (EBG) structures are employed to increase the gains of the antenna at high frequencies. The strip-loaded wide slot antenna (SWSA) is used to stabilize the radiation pattern across the whole operating frequency band in [11]. However, although the radiation pattern at high frequencies is improved to some extent, the cross-polarization of the antennas is in high level in the H-plane, thus the polarization purity still need to be improved.

In order to reduce the cross polarization, which is caused by the transverse currents of higher-order mode, some efforts have been made by researchers [12]. It is found that higher-order mode, especially higher-odd-mode, can be greatly suppressed when the antenna is symmetrically driven using differential feeding systems [13, 14]. Hence, in this study, a compact differential-fed microstrip antenna is presented

Received 8 June 2014, Accepted 5 August 2014, Scheduled 18 August 2014

* Corresponding author: Junhui Wang (xidian_wjh@163.com).

The authors are with the Laboratory of Science and Technology on Antennas and Microwaves, Xidian University, Xi'an, Shaanxi 710071, China.

and analyzed for UWB applications. Furthermore, due to the differential feeding technique, the balun is not needed when the antenna is driven using differential signals [15] in the differential communication applications. An antenna prototype is fabricated to validate the proposed design strategy. The measured results indicates that the designed antenna exhibits a wideband performance from 3 to 12 GHz for $|S_{d11}| < 10$ dB. More importantly, over the entire UWB band, the proposed antenna presents stable omnidirectional radiation patterns in H-plane, with dipole-like radiation patterns in E-plane. By employing differential feeding systems, the cross-polarization level is kept low across the whole operating frequencies, which results in high polarization purity of the antenna.

2. ANTENNA CONFIGURATION

Figure 1 shows the configuration of the proposed antenna which is printed on FR4 substrate with thickness of 1 mm, relative dielectric constant of 4.4, and loss tangent of 0.02. On the top side of the substrate, the differential microstrip feeding lines are etched, loading with two partially cut elliptical patches. The width of the feeding lines are set as 1.86 mm to achieve the characteristic impedance of 50 Ω. For good impedance matching, part of the feeding lines taper from 1.86 to 1 mm. The ground plane is printed on the bottom side of the substrate, and the central part of it is cut by a hexagon-shaped slot. A narrow strip is added along the symmetrical line of the antenna, which divides the slot hexagon into two trapezoid slots. That strip, acting as the virtual ground plane, will somewhat reduce the asymmetrical effect. Also, four corners of the ground plane are cut to ameliorate the impedance matching in the high frequency band. The proposed differential-fed antenna has a compact size of 22 mm × 30 mm. Based on the optimized parameters on Table 1, an antenna prototype is designed and fabricated.

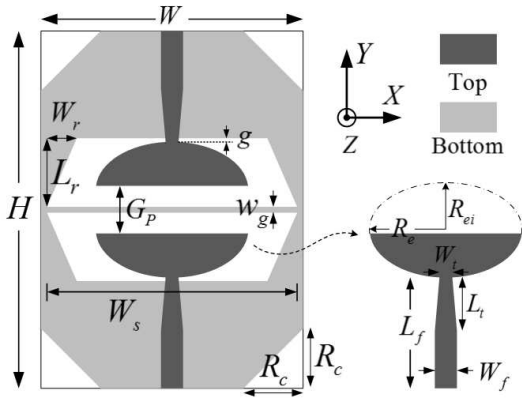

Figure 1. Geometry of the proposed differential-fed antenna.

Table 1. Optimized antenna parameters.

Parameter	W	H	W_S	W_r	L_r	R_c	w_g	g
Value (mm)	22	30	21	2.5	5.75	5	0.5	0.5
Parameter	G_p	R_e	R_{ei}	L_f	W_f	L_t	W_t	
Value (mm)	4	6.4	4	9.5	1.86	4.5	1.1	

3. ANTENNA DESIGN AND ANALYSIS

3.1. Evolve Process of the Proposed Antenna

The evolving process of designing the proposed antenna is shown in Fig. 2. Fig. 3 shows the simulated $|S_{11}|$ results of Ant I and II, which indicates both of them satisfy the impedance matching for the

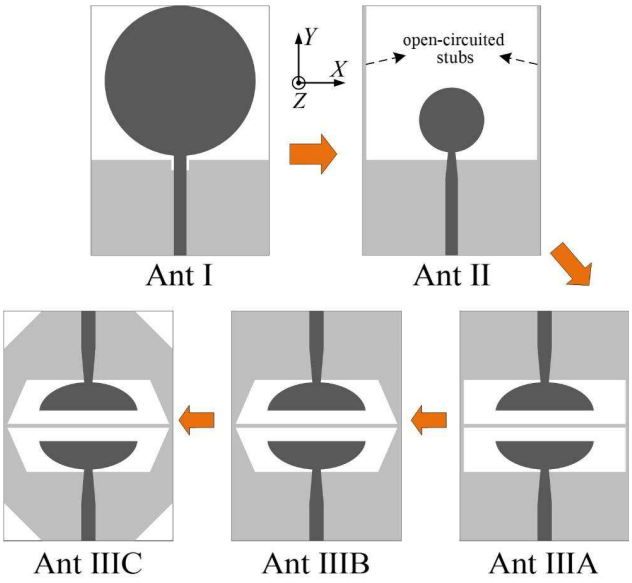

Figure 2. Evolve process of the proposed antennas.

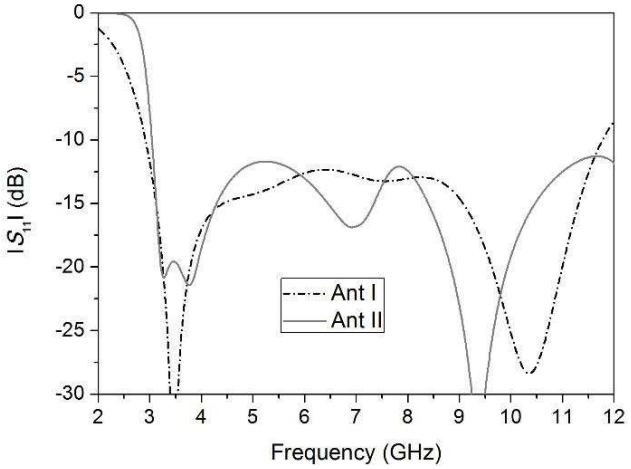

Figure 3. Simulated $|S_{11}|$ results of Ant I and II.

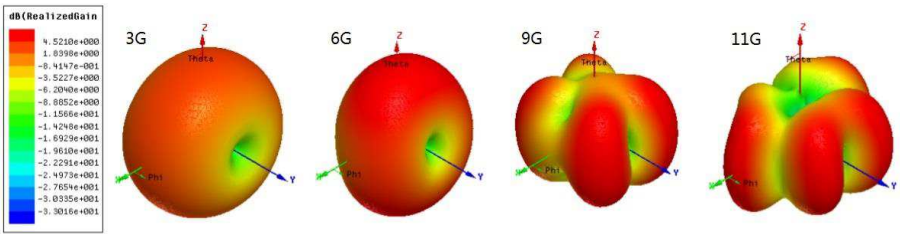

Figure 4. Simulated 3D radiation patterns of Ant I at 3, 6, 9, and 11 GHz.

entire UWB band (3–11 GHz). Ant I, the conventional circular monopole antenna, mainly comprises a circular radiation patch and a rectangular ground [2]. The corresponding simulated 3D radiation plots are described in Fig. 4. As can be seen, the radiation pattern is greatly distorted at high frequencies. At 9 and 11 GHz, a null even appears in the main broadside direction (Z-direction), and the main beam deviated from the direction. To solve that problem, a novel modified planar UWB antenna (Ant II) is presented. It can be seen that the circular patch of Ant II is much smaller than that of the conventional one, while a pair of symmetrical parallel open-circuited stubs is extended from the ground plane. The simulated surface current of the Ant II at 11 GHz is shown in Fig. 5. It can be observed that a significant amount of current is distributed in the symmetrical open-circuited stubs, which can greatly improves the radiation patterns of the antenna at high frequencies. Fig. 6 shows the simulated 3D radiation plots of the modified antenna, which indicate that, at high frequencies, the main beam of the radiation pattern returns back to the broadside direction with the help of the two open-circuited stubs. Also, the simulated radiation patterns in the E-plane and H-plane are shown in Fig. 7. It indicates that, compared with the conventional antenna, the modified UWB antenna reveals an improved radiation characteristics at high frequencies. However, the cross-polarization level is a little high at high frequencies, especially compared with the co-polarization in the H-plane.

To improve the radiation polarization purity in the high frequency band, the strategy of differentially driven systems is introduced, and the differential-fed Ant IIIA, IIIB, and IIIC are presented. A differential-fed antenna can be regarded as a differential two-port network. Thus, the differential reflection coefficient of the antenna can be defined as

$$S_{d11} = \frac{1}{2}(S_{11} - S_{12} - S_{21} + S_{22})$$

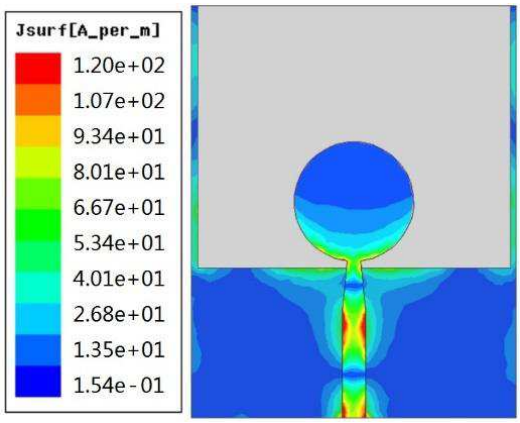

Figure 5. Simulated surface current distribution of Ant II at 11 GHz.

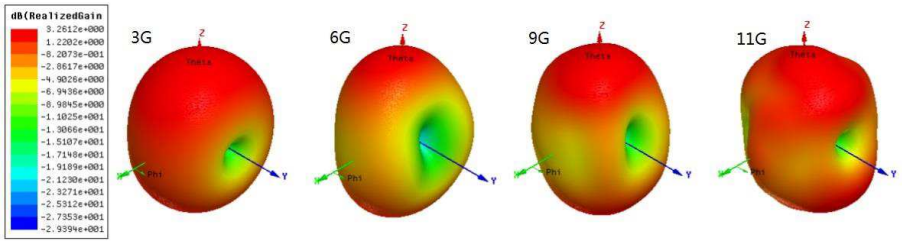

Figure 6. Simulated 3D radiation patterns of Ant II at 3, 6, 9, and 116,GHz.

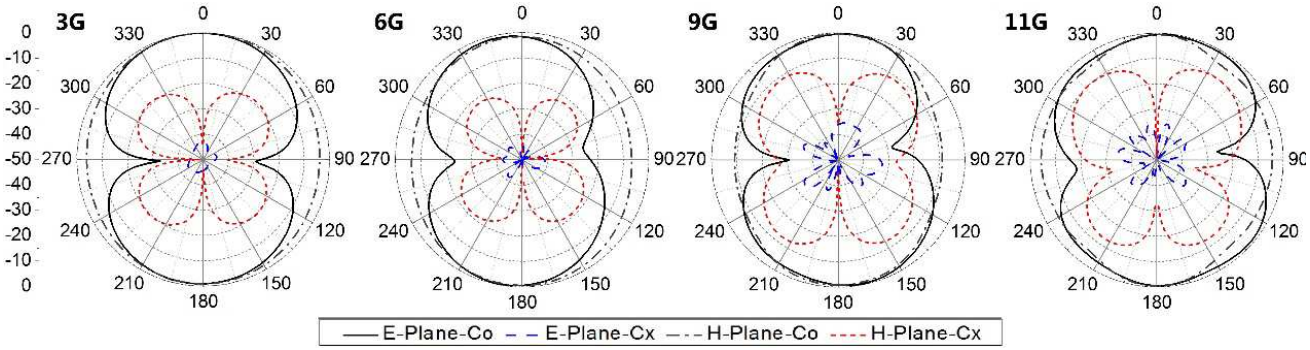

Figure 7. Simulated E- and H-plane radiation patterns of Ant II at 3, 6, 9, and 11 GHz.

which is equivalent to reflection coefficient of the input port of a perfect 180° divider, while the two output ports are connected to the two input ports of the differential-fed antenna. Fig. 8 shows the simulated active $|S_{d11}|$ results for Ant IIIA, IIIB, and IIIC. It can be seen that the impedance matching of Ant IIIA in both low and high frequency bands is terrible. Compared with Ant IIIA, four symmetrical triangles are added along the edge stubs of Ant IIIB. The simulated results indicates that, in the low frequency band, the impedance matching of Ant IIIB is greatly improved with the addition of four triangle patches. To further improve the impedance matching at high frequencies, four symmetrical isosceles right triangles are cut from the corners of ground plane. Finally, the differential-fed microstrip antenna (Ant IIIC), with ultra-wide impedance band of 3–12 GHz for $|S_{d11}| < 10$ dB, is proposed.

To describe the radiation characteristics of proposed Ant IIIC, the simulated 3D radiation plots are shown in Fig. 9. It can be observed that the main beams of the proposed antenna are stabilized in the broadside direction. To validate the effect of the differential feeding systems, the simulated 2D radiation patterns (E- and H-planes) at 3, 6, 9, and 11 GHz are plotted in Fig. 10. Obviously, it can be

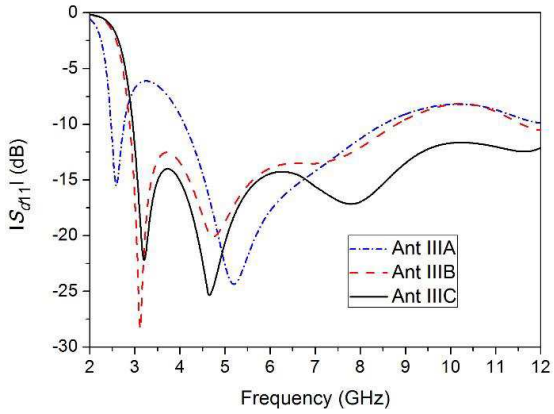

Figure 8. Simulated $|S_{11}|$ results of Ant IIIA, IIIB, and IIIC.

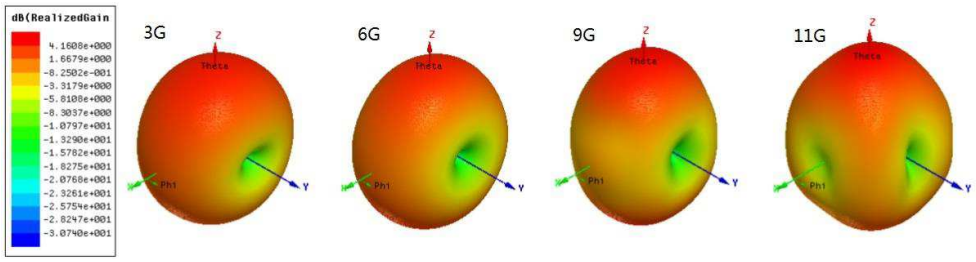

Figure 9. Simulated 3D radiation patterns of the proposed antenna (Ant IIIC) at 3, 6, 9, and 11 GHz.

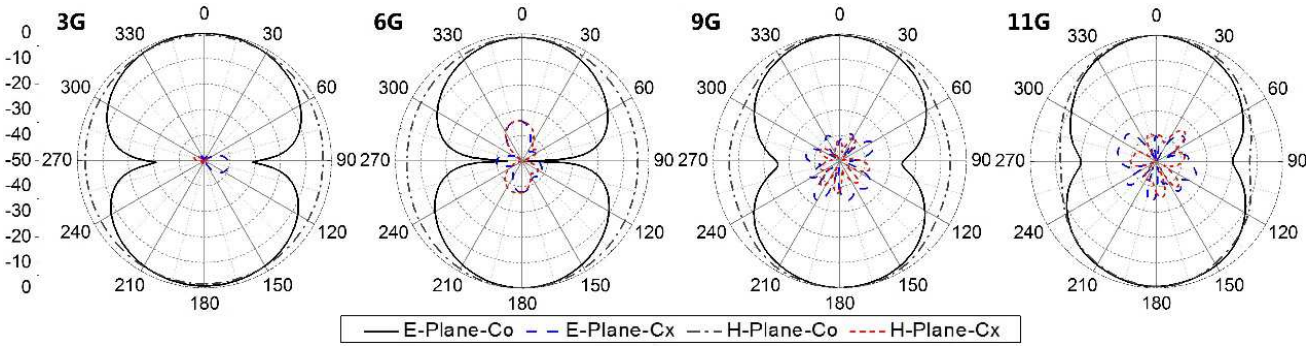

Figure 10. Simulated E- and H-plane radiation patterns of the proposed antenna (Ant IIIC) at 3, 6, 9, and 11 GHz.

seen that the proposed antenna displays stable omnidirectional radiation patterns in the H-plane and dipole-like radiation patterns in the E-plane across the entire operating frequencies. Most important of all, the cross-polarization levels are greatly reduced compared with that of Ant I and II, especially in the high frequency band. Therefore, due to the employment of the differentially driven strategy, the polarization purity of the proposed antenna (Ant IIIC) is greatly improved.

3.2. Key Parameter Study of the Proposed Antenna

To further analyze the structure of the proposed antenna, some key parameters are simulated and discussed. It should be noted that, when one parameter varies, the others are kept unchanged. Fig. 11 shows the simulated $|S_{d11}|$ results with different values of W_r, one side length of the added triangles.

It can be found that the first resonant frequency shifts from 3 to 3.38 GHz as W_r increases from 2 to 4 mm, which leads to the improvement of impedance matching in the low frequency band. However, with the decreasing of side length W_r, the lowest operating frequency edge increases and the impedance BW may become narrower. The simulated results according to variation of R_c is illustrated in Fig. 12. It indicates that increasing R_c would improve the impedance matching at high frequencies; meanwhile,

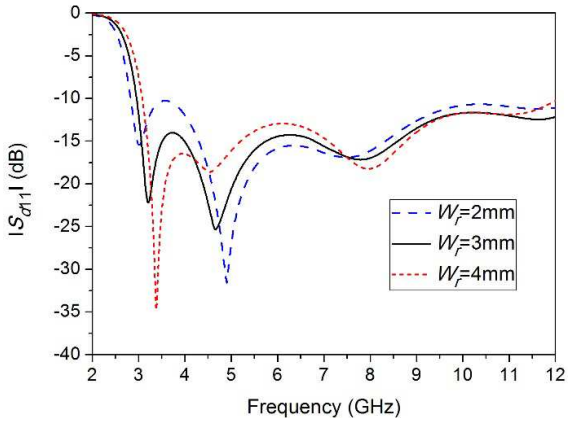

Figure 11. Simulated $|S_{d11}|$ results of proposed antenna with variation of parameter W_r.

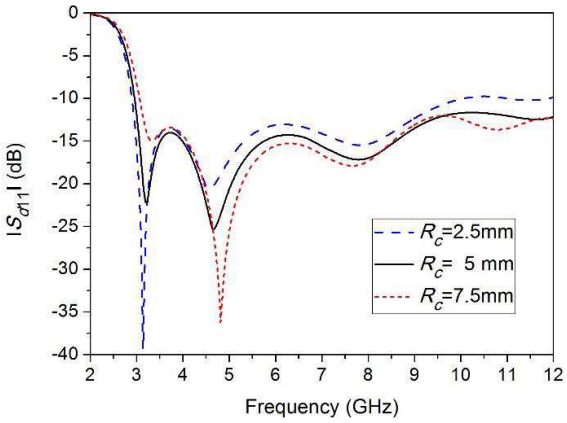

Figure 12. Simulated $|S_{d11}|$ results of proposed antenna with variation of parameter W_c.

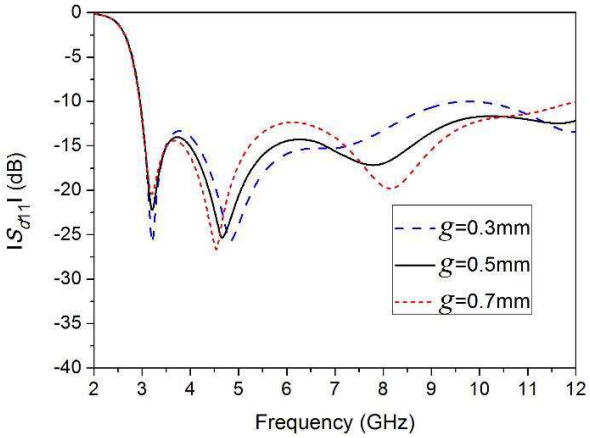

Figure 13. Simulated $|S_{d11}|$ results of proposed antenna with variation of parameter g.

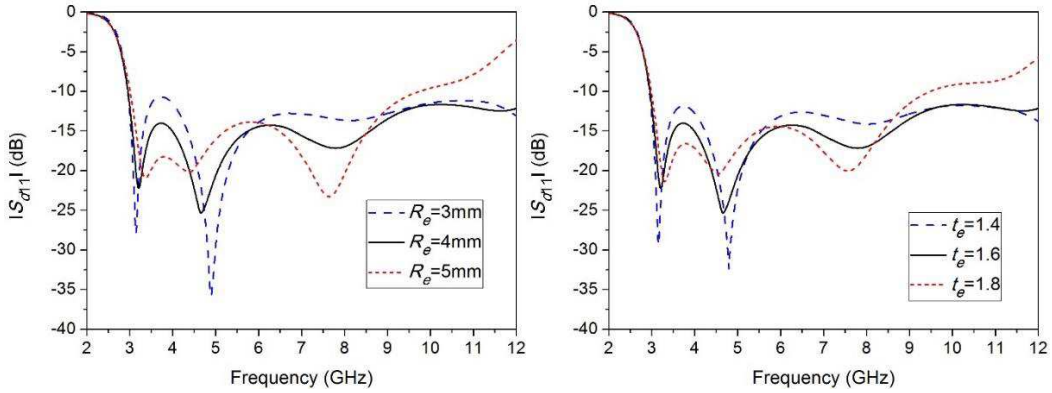

(a) (b)

Figure 14. Simulated $|S_{d11}|$ results of proposed antenna with variation of parameter (a) R_e and (b) t_e.

it shifts the lowest operating frequency higher. Thus, the optimal side length ($R_c = 4\,\text{mm}$) of the triangle cut in the corner is selected, which guarantee the $|S_{d11}|$ is lower than $-10\,\text{dB}$ over the entire UWB frequency band. Also, the gap (g) between elliptical patch and the ground plays an important role for the impedance matching of the proposed antenna. Fig. 13 shows the simulated $|S_{d11}|$ results with different values of g, which indicates optimal impedance matching can be achieved when g equals to 0.5 mm. The simulated results with various minor axis R_e and various axis ratio t_e ($t_e = R_e/R_{ei}$) are shown in Figs. 14(a) and (b). It can be see that the impedance matching from 3 to 12 GHz is greatly improved when $R_e = 4\,\text{mm}$ and $t_e = 1.6$.

4. MEASUREMENT RESULTS AND DISCUSSION

Based on the optimized parameters of the proposed differential-fed UWB antenna, the antenna prototype was fabricated on a FR4 substrate. An Agilent N5230A vector network analyzer was used to measure the S-parameters: S_{11}, S_{22}, S_{12}, and S_{21} for the proposed antenna. Then the differential reflection coefficient $|S_{d11}|$ can be obtained using the Equation (1). Fig. 15 displays the simulated and measured results of the designed antenna. It can be observed that the fabricated antenna achieved a wideband performance from 3.1 to 12 GHz for $|S_{d11}| < -10\,\text{dB}$. The discrepancy between measured and simulated results is probably owing to the fluctuation of the dielectric constant or tolerance in process.

In the pattern measurement, because the differentially feeding signal is hard to be implemented

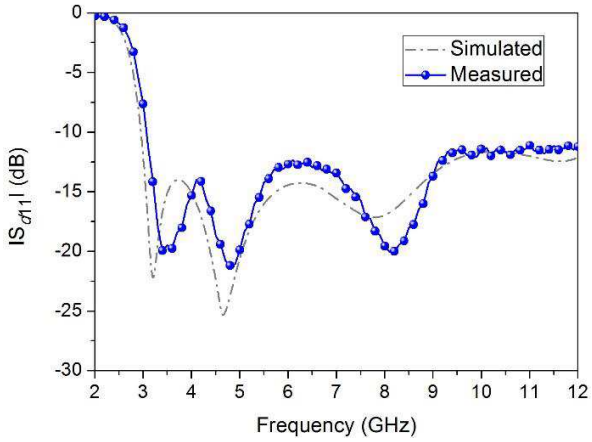

Figure 15. Measured $|S_{d11}|$ results of the proposed antenna.

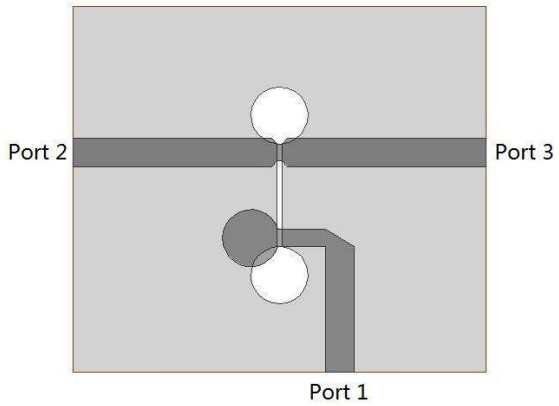

Figure 16. Geometry of the wideband out-of-phase power divider.

Figure 17. Photo of the proposed antenna connected with the out-of-phase power divider.

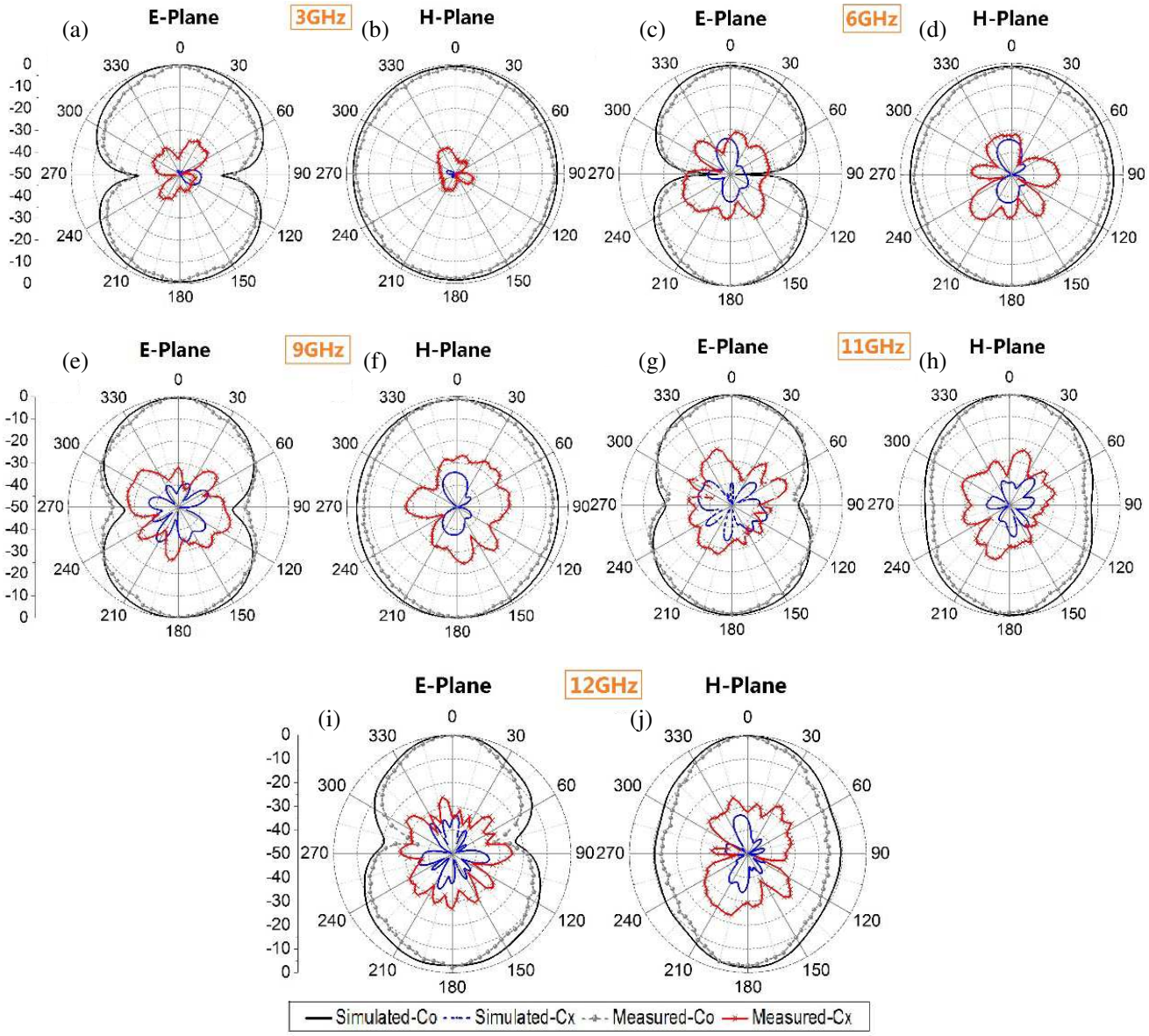

Figure 18. Simulated and measured radiation patterns of the proposed antenna: E-plane at (a) 3, (c) 6, (e) 9, (g) 11, and (i) 12 GHz; H-plane at (b) 3, (d) 6, (f) 9, (h) 11, and (j) 12 GHz.

directly, a wideband out-of-phase power divider as shown in Fig. 16 is used to measure the radiation characteristics of the differentially driven antenna [16]. As shown in Fig. 17, the two 180° output ports (Port 2 and Port 3) of the divider are connected to the two inputs of the designed antenna. The measured radiation patterns in E- and H-planes at 3, 6, 9, 11, and 12 GHz are plotted in Fig. 18. It can be seen that, over the whole UWB band, the proposed antenna exhibits a stable omnidirectional radiation pattern in the H-plane and dipole-like radiation pattern in the E-plane, and the main beams are consistently stabilized on the broadside direction. Moreover, the measured cross-polarization level of the designed antenna are lower than −20 dB in the entire frequency band. Compared with the antennas aforementioned [2–7, 10, 11], the polarization purity of the proposed antenna is greatly improved. Fig. 19 shows the simulated and measured gains in the broadside direction. It can be observed that the measured gain variation of the proposed antenna is confined between 2.7 and 4.5 dB, indicating very stable gains compared with the conventional circular monopole antenna (Ant I). All the disagreement above between the simulated and measured results may be result from the imperfect of the anti-phase power divider.

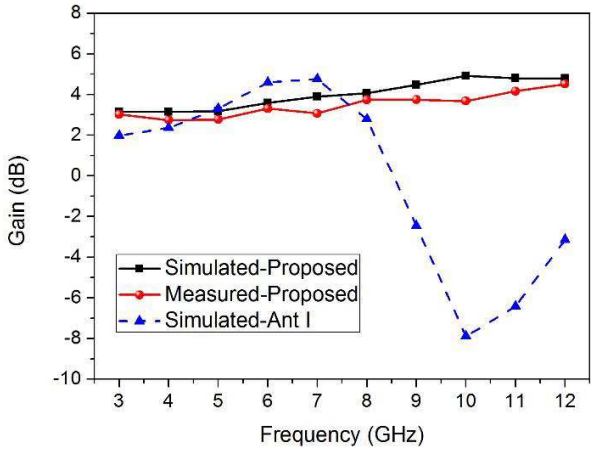

Figure 19. Simulated and measured gains of the proposed antenna.

5. CONCLUSION

In this study, a compact differential-fed microstrip antenna is presented for UWB communication systems. Due to the symmetrical trapezoid shaped slot on central of the ground plane, the impedance matching is greatly improved in the low frequency band. To further ameliorate the impedance matching at high frequencies, four symmetrical right triangles are cut from the four corners of the ground plane. More importantly, the proposed antenna reveals a stable omnidirectional radiation patterns over the entire UWB frequency band. Meanwhile, due to the differentially driven systems, the cross-polarization is maintained in a low level from 3 to 12 GHz, and polarization purity is high even a. Therefore, the compact size, simple structure, and improved radiation property make the proposed antenna a good candidate for various UWB utilizations.

REFERENCES

1. Federal Communication's Commission, Washington, DC, "Revision of part 15 of the commission's rules regarding ultra-wideband transmission systems, First note and order," ET-Docket 98-153, 2002.
2. Liang, J. X., C. C. Chiau, X. D. Chen, and C. G. Parini, "Study of a printed circular disc monopole antenna for UWB systems," *IEEE Trans. Antennas Propag.*, Vol. 53, No. 11, 3500–3504, 2005.
3. Lin, Y. C. and K. J. Hung, "Compact ultrawideband rectangular aperture antenna and band-notched designs," *IEEE Trans. Antennas Propag.*, Vol. 54, No. 11, 3075–3081, 2006.
4. Sim, C.-Y.-D., W. T. Chung, and C. H. Lee, "Compact slot antenna for UWB applications," *IEEE Antennas Wireless Propag. Lett.*, Vol. 9, 63–66, 2010.
5. Li, D. T. and J. F. Mao, "A koch-like sided fractal bow-tie dipole antenna," *IEEE Trans. Antennas Propag.*, Vol. 60, No. 5, 2242–2251, 2012.
6. Huang, X. D., C. H. Cheng, and L. Zhu, "An ultrawideband (UWB) slotline antenna under multiple-mode resonance," *IEEE Trans. Antennas Propag.*, Vol. 60, No. 1, 385–389, 2012.
7. Sayidmarie, K. H. and Y. A. Fadhel, "A planar self-complementary bow-tie antenna for UWB applications," *Progress In Electromagnetics Research C*, Vol. 35, 253–267, 2013.
8. Fereidoony, F., S. Chamaani, and S. A. Mirtaheri, "Systematic design of UWB monopole antennas with stable omnidirectional radiation pattern," *IEEE Antennas Wireless Propag. Lett.*, Vol. 11, 752–755, 2012.
9. Touhami, N. A., Y. Yahyaoui, A. Zakriti, K. Bargach, M. Boussouis, M. Lamsalli, and A. Tribak, "A compact CPW-Fed planar pentagon antenna for UWB applications," *Progress In Electromagnetics Research C*, Vol. 46, 153–161, 2014.

10. Fereidoony, F., S. Chamaani, and S. A. Mirtaheri, "UWB monopole antenna with stable radiation pattern and low transient distortion," *IEEE Antennas Wireless Propag. Lett.*, Vol. 10, 302–305, 2011.
11. Qu, S., J. Li, J. Chen, and Q. Xue, "Ultra wideband strip-loaded circular slot antenna with improved radiation patterns," *IEEE Trans. Antennas Propag.*, Vol. 55, No. 11, 3348–3353, 2007.
12. Sim, C., C.-C. Chang, and J.-S. Row, "Dual-feed dual-polarized patch antenna with low cross polarization and high isolation," *IEEE Trans. Antennas Propag.*, Vol. 57, No. 10, 3321–3324, 2009.
13. Zhang, Y. P. and J. J. Wang, "Theory and analysis of differentially-driven microstrip antennas," *IEEE Trans. Antennas Propag.*, Vol. 54, No. 4, 1092–1099, 2006.
14. Tong, Z., A. Stelzer, and W. Menzel, "Improved expressions for calculating the impedance of differential feed rectangular microstrip patch antennas," *IEEE Microw. Wireless Compon. Lett.*, Vol. 22, No. 9, 441–443, 2012.
15. Han, L. P., W. M. Zhang, X. W. Chen, G. R. Han, and R. B. Ma, "Design of compact differential dual-frequency antenna with stacked patches," *IEEE Trans. Antennas Propag.*, Vol. 58, No. 4, 1387–1392, 2010.
16. Bialkowski, M. E. and A. M. Abbosh, "Design of a compact UWB out-of-phase power divider," *IEEE Microw. Wireless Compon. Lett.*, Vol. 17, No. 4, 289–291, 2007.